An Analytical Carrier Recombination Turn-Off Transient Model for High-Voltage IGBTs

Zhiyuan Zhang, Hengxin He, *Member, IEEE*, Kejie Li, *Member, IEEE*, Nianwen Xiang, *Member, IEEE*, and Weijiang Chen, *Senior Member, IEEE*

***Abstract*—High-voltage insulated-gate bipolar transistors (IGBTs) have been extensively used in power electronic systems, such as railway traction inverters, flexible dc transmission systems, and wind turbines, and it is necessary to investigate transient modeling of high-voltage IGBTs. Based on the mechanism of the switching transient, this article proposes a new analytical model for the turn-OFF process of high-voltage IGBTs. First, considering the large base width of high-voltage IGBTs, the defect of the first-order approximation assumptions used in the existing model is analyzed in detail. Then, by using hyperbolic approximation, an improved solution method is developed for the transient ambipolar diffusion equation that considers the influence of carrier recombination in the base region. Finally, the accuracy of the proposed method is verified by comparing its simulation results with the experiment data obtained under the double pulse circuit. Results show that the proposed analytical model can more accurately simulate switching behaviors in the turn-OFF process.**

***Index Terms*—Ambipolar diffusion equation (ADE), analytical transient model, high-voltage, hyperbolic approximation, insulated-gate bipolar transistor (IGBT), turn-OFF process.**

NOMENCLATURE

A	Device area (cm^2).
b	Mobility ratio in the base.
b_H	Mobility ratio in the field-stop layer.
C_{bc}	base-collector depletion capacitance (F).
D	$=2D_nD_P/(D_n+D_P)$ Ambipolar diffusivity in the base (cm^2/s).
D_H	$=2D_{nH}D_{PH}/(D_{nH}+D_{PH})$ Ambipolar diffusivity in the field-stop layer (cm^2/s).
$D_{n,\ p}$	$=\mu_{n,p}kT/q$ Electron and hole diffusivity in the base (cm^2/s).
$D_{nH,\ pH}$	$=\mu_{nH,pH}kT/q$ Electron and hole diffusivity in the field-stop layer (cm^2/s).
E_{Fn}	Fermi energy level of electrons (J).
E_{Fp}	Fermi energy level of holes (J).
E_{Fi}	Quasi-Fermi potential (J).
I_{mos}	MOS channel current (A).
I_n	Electron current in the base (A).
I_p	Hole current in the base (A).
I_{nH}	Electron current in the field-stop layer (A).
I_{pH}	Hole current in the field-stop layer (A).
I_{sne}	Emitter electron saturation current (A).
I_T	Anode current (A).
L	Diffusion length in the base (cm).
L_H	Diffusion length in the field-stop layer (cm).
K_p	MOS channel transconductance (A/V^2).
n	Electron concentration in the base (cm^{-3}).
δn	Excess electron concentration in the base (cm^{-3}).
n_H	Electron concentration in the field-stop layer (cm^{-3}).
δn_H	Excess electron concentration in the field-stop layer (cm^{-3}).
n_i	Intrinsic carrier concentration (cm^{-3}).
N_B	Base doping concentration (cm^{-3}).
N_H	Field-stop layer doping concentration (cm^{-3}).
p	Hole concentration in the base (cm^{-3}).
p_C	Charge control component in the base (cm^{-3}).
p_H	Hole concentration in the field-stop layer (cm^{-3}).
δp	Excess hole concentration in the base (cm^{-3}).
δp_H	Excess hole concentration in the field-stop layer (cm^{-3}).
P_{L0}	Hole concentration at $x=0$ (cm^{-3}).
P_{H0}	Hole concentration at $x_H=0$ (cm^{-3}).
P_{HW}	Hole concentration at $x_H=W_H$ (cm^{-3}).
Q	Unit electron charge ($=1.6\times10^{-19}$ C).
Q	Total carrier charge (C).
Q_L	Charge stored in the base region (C).
Q_H	Charge stored in the field-stop layer charge (C).
τ	Lifetime in the base (s).
τ_H	Lifetime in the field-stop layer (s).
T	Junction temperature (K).
$\mu_{n,p}$	Electron and hole mobility in the base (cm^2/V·s).
$\mu_{nH,pH}$	Electron and hole mobility in the field-stop layer (cm^2/V·s).
V_{AC}	IGBT anode-cathode voltage (V).
V_{bc}	Base-collector voltage (V).
V_{bi}	Built-in junction potential (V).

Manuscript received 24 August 2023; revised 19 January 2024; accepted 8 March 2024. Date of publication 13 March 2024; date of current version 19 April 2024. This work was supported in part by the National Natural Science Foundation of China under Grant 51977090 and in part by the National Key R&D Program of China under Grant 2021YFB2401100. Recommended for publication by Associate Editor J. Popovic-Gerber. *(Corresponding author: Hengxin He.)*

Zhiyuan Zhang and Hengxin He are with the State Key Laboratory of Advanced Electromagnetic Engineering and Technology, Huazhong University of Science and Technology, Hubei 430074, China (e-mail: d201880441@hust.edu.cn; hengxin_he@hust.edu.cn).

Kejie Li and Nianwen Xiang are with the School of Electrical and Automation Engineering, Hefei University of Technology, Anhui 230000, China (e-mail: kejie.li@hfut.edu.cn; xiangnianwen@hfut.edu.cn).

Weijiang Chen is with the State Grid Corporation of China, Beijing 100000, China (e-mail: weijiang-chen@sgcc.com.cn).

Color versions of one or more figures in this article are available at https://doi.org/10.1109/TPEL.2024.3377000.

Digital Object Identifier 10.1109/TPEL.2024.3377000

V_{eb} Emitter–base junction voltage (V).
V_{gs} IGBT gate-cathode voltage (V).
$\varphi_{nej,pej}$ Quasi-Fermi potentials of electrons and holes at anode-base junction (V).
V_T Threshold voltage (V).
W Quasi-neutral base width (μm).
W_b Base width (μm).
W_{bc} Base-collector depletion width (μm).
W_H Field-stop layer width (μm).

I. Introduction

INSULATED-GATE bipolar transistors (IGBTs) are widely used in power electronic systems (PESs) of industry applications such as wind turbines. Railway traction inverters, and flexible dc transmission systems [1], [2]. With the rapid development of new energy generation, flexible dc transmission systems, and electric vehicles, IGBTs have become the most critical switching power semiconductor in high-voltage systems [3], [4]. An accurate transient IGBT model is the key to the design of the devices and systems [5]. This article focuses on modeling the turn-OFF process, which helps to predict the electromagnetic compatibility problem, overvoltage problem, and switching loss [6], [7], [8].

Existing IGBT models can be classified into behavior models and physical models [9]. When behavior models are applied to the design and transient analysis of systems, they are not sufficient and must be substituted by physical models, which can not only achieve high accuracy but also support a detailed analysis of the transient process [10].

In recent years, many physical models have been proposed, such as the Hefner model, the lumped charge model, the Fourier-series-based (FSB) model, etc. The effects of conductivity modulation on the terminal characteristics of a semiconductor device were analyzed without considering the influence of moving boundaries in the transient process [11], [12]. Transient characteristics of Schottky injection FETs were investigated based on two-dimensional (2-D) numerical simulations [13], [14]. Hefner proposed the first-order approximation to establish a transient model based on the analysis of the effect of the moving depletion edge boundary [15], [16]. Based on this, Ji et al. [17], [18] considered the influence of carrier concentration on carrier lifetime. Based on the first-order approximation, Luo et al. [19] took the carrier recombination in the base region and the injection level in the buffer layer into consideration, which was ignored by Hefner in the analysis. Kraus and Hoffmann adopted a polynomial distribution to approximate the transient carrier concentration [20], [21]. Lauritzen and Ma [22] proposed the lumped charge model for power devices. Iannuzzo and Busatto [23] modified the lumped charge method and presented a more general methodology for implementing the model into a circuit form. Duan et al. [24], [25] improved the accuracy of the lumped-charge IGBT model. Leturcq et al. [26] first proposed to employ the Fourier transform to solve the ambipolar diffusion equation (ADE). Then, Palmer applied the method to IGBT and constructed the FSB IGBT model and continuously improved it [27], [28], [29], [30]. Liu et al. [31], [32] investigated the extraction method of the parameters of the FSB model. Bonyadi et al. [33] further considered the 2-D effect. Xue et al. [34] employed the Fourier-series solution of ADE at all injection levels to characterize the excess carrier transport in the N-base.

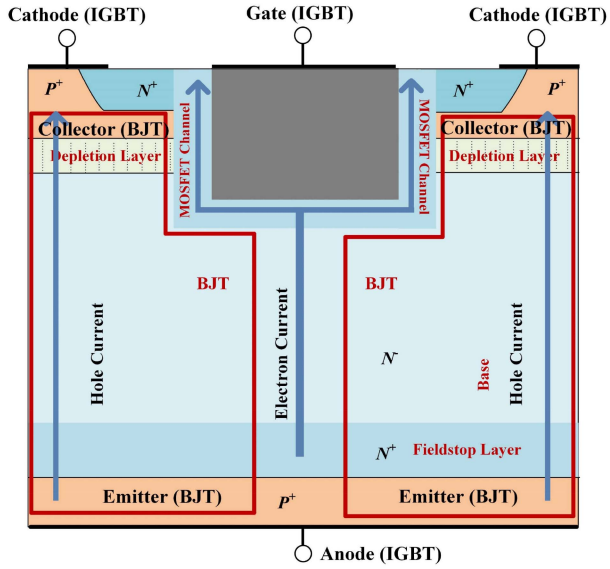

Fig. 1. Diagram of the high-voltage IGBT structure (conduction state).

Among the existing models, the FSB model and the lumped charge model perform Fourier transform and simplification based on the point-charge assumption for the carriers. However, the parameters in the FSB model do not have practical physical significance. The lumped charge model cannot be used to analyze the carrier transport process and has some defects in convergence. In contrast, the Hefner model does have the non-convergence problem, and all the parameters in the model have physical significance.

Nevertheless, the Hefner model is established for middle-to-low voltage IGBTs, and the recombination of carriers is ignored in the model. For the high-voltage IGBT (Infineon, 1.7 kV), the base width is much higher than the ambipolar diffusion length. In this case, the recombination of carriers cannot be ignored, and the first-order approximation of the Hefner model is not applicable. Therefore, it is necessary to analyze the special characteristics of the high-voltage IGBT in the turn-OFF process and establish a transient model suitable for the high-voltage IGBT.

In this article, a new analytical transient model is proposed for analyzing the turn-OFF process of high-voltage IGBTs. Compared with the existing models, the proposed model adopts a hyperbolic approximation of carrier distribution to make it more suitable for high-voltage IGBT.

The rest of this article is organized as follows. In Section II, the defects of the existing first-order approximation are analyzed, and the proposed transient model is introduced. In Section III, the accuracy of the proposed model is verified based on the experimental data. Finally, Section IV concludes this article.

II. Model Description

Fig. 1 shows the structure of the common high-voltage IGBT, with special structures such as the field-stop layer and the

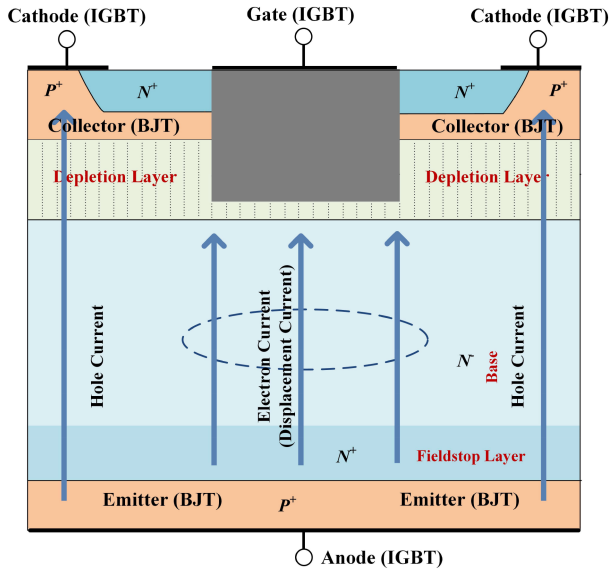

Fig. 2. Ambipolar diffusion process of carriers in the base and field-stop region in the turn-OFF stage.

trench gate. The IGBT can be regarded as a composite structure composed of a metal-oxide-semiconductor field-effect transistor (MOSFET) and a bipolar junction transistor (BJT). The MOSFET provides a gate drive current for the BJT. To distinguish from BJT terminals, the high-voltage and low-voltage terminals of the IGBT are marked as anode and cathode. The anode and cathode of the IGBT are the emitter and collector of the BJT, respectively. The ambipolar diffusion of the carriers in the base determines the performance of the IGBT, and the MOSFET channel formed below the gate provides the most carriers for the recombination in the base.

To turn OFF the IGBT, the gate voltage decreases rapidly below the threshold voltage, which removes the MOSFET channel quickly. Meanwhile, the IGBT slowly consumes excess carriers stored in the base region and the field-stop layer, and this is the main process in the turn-OFF stage. It should be noted that the regions near the cathode and gate will be covered by the depletion layer in a very short time, as shown in Fig. 2. Therefore, the trench gate structure has little impact on the turn-OFF process and is not considered in this article. The carrier transport process in the base region and the field-stop layer can be approximately considered to be 1-D in the turn-OFF stage, as shown in Fig. 3.

The base region can be divided into the quasi-neutral region and the depletion region. The voltage drop in the depletion layer accounts for most of the IGBT anode-cathode voltage ($V_{AC} = V_{bc}$) in the turn-OFF stage. In the transient process, the boundary of the depletion layer moves as the anode-cathode voltage changes. Meanwhile, the ambipolar diffusion process in the quasi-neutral region and the field-stop layer transports electrons generated by the movement of the base-collector depletion region. Thus, to model the turn-OFF behavior, the key is to analyze the bipolar transport processes in the neutral region and the field-stop layer under the moving boundary. In the conduction state, the carrier distribution can be obtained by solving the steady-state ADE, which is a hyperbolic function.

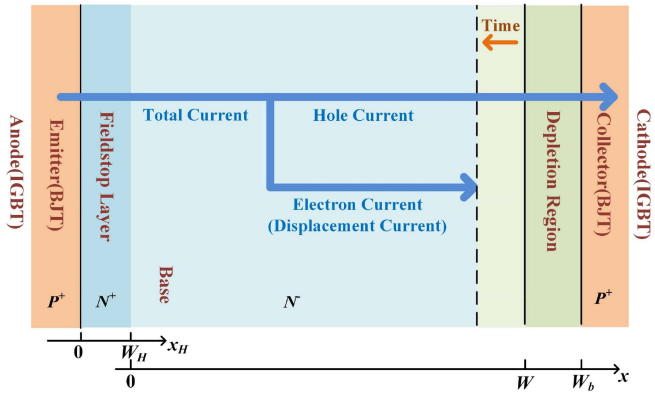

Fig. 3. Coordinate system used in bipolar transistor base modeling.

However, under a moving boundary, the transient ADE cannot be solved analytically, making it difficult to model the transient process.

Under the high-injection condition ($\delta n + N_B = \delta p + n_i^2/N_B \approx n = p$), the transport of carriers in the neutral region can be described accurately by the ADE

$$\frac{\partial^2 p}{\partial x^2} = \frac{p}{L^2} + \frac{1}{D}\frac{\partial p}{\partial t}. \tag{1}$$

In the switching transient process, the anode-cathode voltage V_{AC} changes continuously, and the width of the depletion layer changes accordingly, so the ambipolar diffusion in the neutral region can be formulated as a moving boundary problem (MBP). Solving this MBP is the most important part of modeling the transient process.

A. The Inadequacy of the Existing First-Order Approximation

The Hefner model is established for middle-to-low voltage IGBTs, where the base width is narrow and much smaller than the ambipolar diffusion length ($W_b \ll L$). Therefore, the recombination of carriers is ignored in the existing models, indicating that the term $\frac{p}{L^2}$ in (1) can be ignored. The ADE can be simplified into the following form:

$$\frac{\partial^2 p}{\partial x^2} = \frac{1}{D}\frac{\partial p}{\partial t}. \tag{2}$$

For the existing models, a solution method has been developed based on first-order approximation (linear approximation) for (2). In this approximation, the carrier distribution is considered to consist of a linear charged control component plus a redistribution component due to the moving boundary of the base-collector depletion region. The redistribution component is assumed to be a small perturbation on the linear distribution, and it only changes the distribution of carriers and does not change the total number of carriers, as illustrated in Fig. 4. This assumption has been proven to be applicable in the narrow base width of middle-to-low voltage IGBTs. However, this linear assumption is not applicable to high-voltage IGBTs.

For high-voltage IGBTs, the base width is much larger than the ambipolar diffusion length ($W_b \gg L$), and the recombination of carriers cannot be ignored during the switching transient,

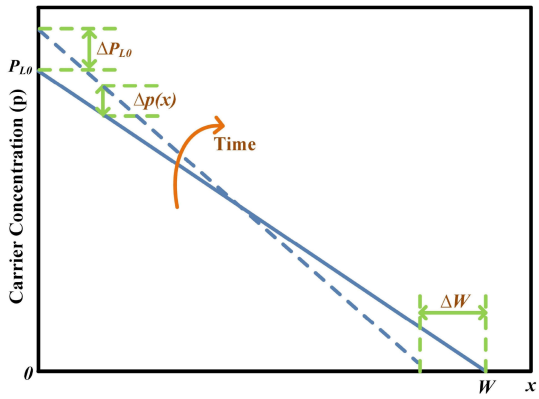

Fig. 4. Distribution of carrier concentration considering the effect of moving boundary of the depletion layer simplified by the first-order approximation.

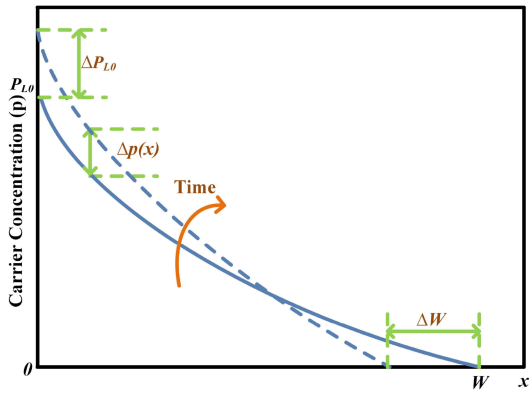

Fig. 5. Distribution of carriers considering the effect of moving boundary simplified by the hyperbolic approximation proposed in this article.

indicating that the term $\frac{p}{L^2}$ in (1) must be considered. By making the existing first-order approximation to (1) and integrating it, p can be obtained as follows:

$$p(x,t) = P_{L0}(t)\left[1 - \frac{x}{W(t)} - \frac{xW(t)}{3L^2} + \frac{x^2}{2L^2} - \frac{x^3}{6L^2W(t)}\right] + \frac{P_{L0}(t)}{D}\frac{dW(t)}{dt}\left[\frac{x}{6} - \frac{x^2}{2W(t)} + \frac{x^3}{3W(t)^2}\right]. \quad (3)$$

Based on the carrier concentration distribution, the charge stored in the base region Q_L can be obtained as follows:

$$Q_L = \int_0^{W(t)} qAp(x,t)\,dx = \frac{qAWP_{L0}(t)}{2}\left(1 - \frac{W^2}{12L^2}\right). \quad (4)$$

It can be seen from (4) that the first-order approximation is not applicable to high-voltage IGBTs mainly for two reasons:

1) In the first-order approximation, it is assumed that the redistribution component only changes the distribution of carriers and does not change the total number of carriers. However, in high-voltage IGBTs, the redistribution component changes the total charge that should be equal to the linear charged control component $(qAWP_{L0}/2)$. After making the first-order approximation to (1), Q_L differs greatly from $qAWP_{L0}/2$, and this contradicts the assumption.
2) For high-voltage IGBTs, the base width is much larger than the ambipolar diffusion length $(W_b \gg L)$, indicating that the value of Q_L calculated by (4) will be negative, and this is incorrect.

Due to the above two reasons, the existing first-order approximation is not suitable for high-voltage IGBTs. Therefore, it is necessary to develop a new method that can be used to solve the ADE under the moving boundary condition for high-voltage IGBTs.

B. Proposed Hyperbolic Approximation

First, the existing first-order approximation is investigated as a reference for the proposed new method. Without considering the effect of the time-varying term, (2) can be transformed into a Laplace equation, and the solution to this equation under the corresponding boundary conditions $[P_L(x=0) = P_{L0}, P_L(x=W) = 0]$ is a linear function. Therefore, existing models adopt the first-order approximation (linear approximation) and assume that the charge control component conforms to linear distribution.

For the high-voltage IGBT, the carrier diffusion equation is shown in (1). In this article, a new approximation is used: the carrier distribution is composed of a charged control component and a redistribution component due to the moving boundary; meanwhile, the redistribution component is assumed to be a small perturbation on the charged control component, which only changes the distribution of carriers and does not change the total number of carriers, as shown in Fig. 5.

The distribution of the charge control component is analyzed first. When the effect of the time-varying term is ignored, (1) can be transformed into Poisson's equation. Under the boundary conditions of the base region $[P_L(x=0) = P_{L0}, P_L(x=W) = 0]$, it is reasonable to assume that the charge control component p_C conforms to the hyperbolic distribution:

$$p_C = P_{L0}\frac{\sinh\left(\frac{W-x}{L}\right)}{\sinh\left(\frac{W}{L}\right)}. \quad (5)$$

The total charge of the charge control component can be obtained:

$$Q_L = \int_0^{W(t)} qAp_C(x,t)\,dx = \frac{qALP_{L0}}{\sinh\left(\frac{W}{L}\right)}\left[\cosh\left(\frac{W}{L}\right) - 1\right] \quad (6)$$

Since the redistribution component only changes the distribution of carriers without changing the total charge, (7) shown at the bottom of next page, must be satisfied. Based on this, ΔP_{L0} and ΔW satisfy the following relationship:

$$\frac{\Delta P_{L0}}{\Delta W} = -\frac{P_{L0}}{L\sinh\left(\frac{W}{L}\right)}. \quad (8)$$

$\frac{\partial p}{\partial t}$ can be obtained from (5) and (8):

$$\frac{\partial p}{\partial t}=\frac{P_{L0}}{L}\frac{\sinh\left(\frac{x}{L}\right)-\sinh\left(\frac{W-x}{L}\right)}{\left[\sinh\left(\frac{W}{L}\right)\right]^{2}}\frac{dW}{dt} \tag{9}$$

The carrier concentration p can be calculated through (1), (5), and (9), as represented in (10) shown at the bottom of this page.

For the ambipolar diffusion, the transport of electrons and holes in the base are described as

$$I_n=\frac{b}{1+b}I_T+qAD\frac{dp}{dx} \tag{11}$$

$$I_p=\frac{1}{1+b}I_T-qAD\frac{dp}{dx}. \tag{12}$$

Therefore, the electron and hole currents in the base region can be calculated by (10)–(12), as expressed by (13) and (14) shown at the bottom of this page. Note that on the right side of (13) and (14), only I_T, P_{L0}, and W are variables, and the rest of the parameters are constants.

The above discussion has completed the analysis and calculation of the distribution of carriers and current components in the quasi-neutral region of the base region. Next, the transport of carriers in the field-stop layer is analyzed. Considering the high-injection condition ($\delta n_H+N_H=\delta p_H+n_i^2/N_H\approx n_H=p_H$), similar to (1), the transport of carriers in the field-stop layer can be represented as follows:

$$\frac{\partial^2 p_H}{\partial {x_H}^2}=\frac{p_H}{{L_H}^2}+\frac{1}{D_H}\frac{\partial p_H}{\partial t}. \tag{15}$$

The excess hole concentrations at the boundaries of the field-stop layer are given as

$$p_H(0,t)=P_{H0}, p_H(W_H,t)=P_{HW}. \tag{16}$$

As demonstrated in Fig. 6, according to the energy band theory, when using the quasi-equilibrium simplification at the boundary between the field-stop layer and the base, the following relationship should be satisfied:

$$P_{HW}(P_{HW}+N_H)=P_{L0}(P_{L0}+N_B). \tag{17}$$

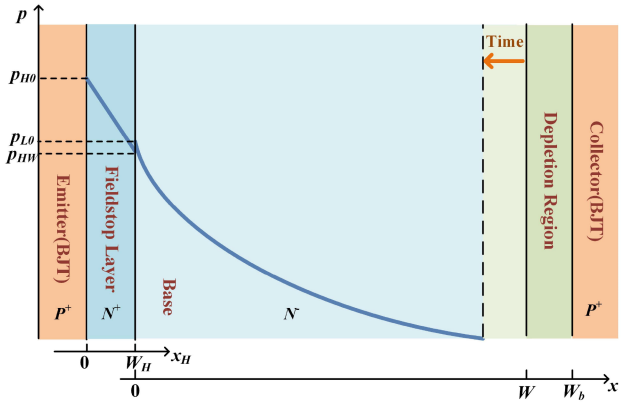

Fig. 6. Schematic diagram of the carrier distribution in the field-stop layer and the base under the moving boundary of the depletion layer.

Since both the field-stop layer and the base region are in a high-level injection state ($P_{HW}\gg N_H, P_{L0}\gg N_B$), (17) can be simplified as

$$P_{HW}=P_{L0}. \tag{18}$$

In the high-voltage IGBT, the field-stop layer is designed to be very thin and has a much smaller length than the ambipolar diffusion length, so it can be assumed that $W_H\ll L_H$. Existing studies have proven that the carriers can be considered to be distributed linearly in the field-stop layer [34], [35]. p_H can be obtained as follows:

$$p_H(x_H,t)=P_{H0}+\frac{P_{HW}-P_{H0}}{W_H}x_H. \tag{19}$$

Based on the distribution of carriers in the field-stop layer, the charge stored in the field-stop layer Q_H can be obtained as follows:

$$Q_H=\int_0^{W_H}qAp_H(x_H,t)\,dx=\frac{qAW_H(P_{HW}+P_{H0})}{2}. \tag{20}$$

The transport of electrons and holes in the field-stop can be also described by (11) and (12). The electron and hole currents

$$\frac{qAL(P_{L0}+\Delta P_{L0})}{\sinh\left(\frac{W+\Delta W}{L}\right)}\left[\cosh\left(\frac{W+\Delta W}{L}\right)-1\right]=\frac{qALP_{L0}}{\sinh\left(\frac{W}{L}\right)}\left[\cosh\left(\frac{W}{L}\right)-1\right]. \tag{7}$$

$$p(x,t)=P_{L0}\frac{\sinh\left(\frac{W-x}{L}\right)}{\sinh\left(\frac{W}{L}\right)}-\frac{P_{L0}L}{D\sinh\left(\frac{W}{L}\right)}\frac{dW}{dt}\left[\frac{\sinh\left(\frac{W-x}{L}\right)-\sinh\left(\frac{x}{L}\right)}{\sinh\left(\frac{W}{L}\right)}+\frac{2x}{W}-1\right]. \tag{10}$$

$$I_n(x,t)=\frac{b}{1+b}I_T-\frac{qADP_{L0}}{L}\frac{\cosh\left(\frac{W-x}{L}\right)}{\sinh\left(\frac{W}{L}\right)}+\frac{qAP_{L0}}{\sinh\left(\frac{W}{L}\right)}\frac{dW}{dt}\left[\frac{\cosh\left(\frac{W-x}{L}\right)+\cosh\left(\frac{x}{L}\right)}{\sinh\left(\frac{W}{L}\right)}-\frac{2L}{W}\right] \tag{13}$$

$$I_p(x,t)=\frac{1}{1+b}I_T+\frac{qADP_{L0}}{L}\frac{\cosh\left(\frac{W-x}{L}\right)}{\sinh\left(\frac{W}{L}\right)}-\frac{qAP_{L0}}{\sinh\left(\frac{W}{L}\right)}\frac{dW}{dt}\left[\frac{\cosh\left(\frac{W-x}{L}\right)+\cosh\left(\frac{x}{L}\right)}{\sinh\left(\frac{W}{L}\right)}-\frac{2L}{W}\right] \tag{14}$$

in the field-stop layer can be obtained, as expressed by

$$I_{nH}(x_H,t) = \frac{b_H}{1+b_H} I_T + qAD_H \frac{P_{HW}-P_{H0}}{W_H} \tag{21}$$

$$I_{pH}(x_H,t) = \frac{1}{1+b_H} I_T - qAD_H \frac{P_{HW}-P_{H0}}{W_H}. \tag{22}$$

Since the current needs to be continuous at the boundary between the field-stop layer and the base, the following relationship should be satisfied:

$$I_{nH}(W_H,t) = I_n(0,t) \tag{23}$$

From (13) and (21), (23) can be transformed into (24) shown at the bottom of this page. Combining (18), P_{H0} and P_{L0} satisfy the relationship expressed in (25) shown at the bottom of this page.

Based on the proposed hyperbolic approximation, the above discussion has completed the analysis and calculation of the distribution of carriers in the base and the field-stop layer in the turn-OFF process. In the following section, the relationship between the anode-cathode voltage $V_{\rm AC}$ and the anode current I_T during the switching transient will be investigated.

C. Relationship Between dV_{AC} and $\mathrm{I_T}$ During the Turn-off Process

It should be noted that in the above analysis, auxiliary variables such as P_{L0}, P_{H0}, and P_{HW} are used to represent the current and concentration of carriers. In the following analysis, these variables variables will be eliminated, and the relational expression containing only three variables I_T, $V_{\rm AC}$, and Q can be obtained. This is a common practice in existing models because it is conducive to the simplification and simulation of the model. During the turn-OFF transient, the voltage drop in the depletion layer between the base and the collector accounts for the majority of the anode-cathode voltage of the IGBT, and it can be approximated that $V_{\rm AC} = V_{bc}$. According to semiconductor physics, the width and voltage of the collector-base depletion layer satisfy the following relationship [36]:

$$W_{bc} = \sqrt{\frac{2\varepsilon_{si}(V_{bi}+V_{bc})}{qN_B}} \approx \sqrt{\frac{2\varepsilon_{si}V_{\rm AC}}{qN_B}}. \tag{26}$$

Based on (26), the relationship between the quasi-neutral base width W and the anode-cathode voltage $V_{\rm AC}$ can be obtained

$$W = W_b - W_{bc} = W_b - \sqrt{\frac{2\varepsilon_{si}V_{\rm AC}}{qN_B}}. \tag{27}$$

Based on (27), $\frac{dW}{dt}$, $\frac{dV_{\rm AC}}{dt}$ and $V_{\rm AC}$ satisfy the following relationship:

$$\frac{dW}{dt} = -\sqrt{\frac{\varepsilon_{si}}{2qN_BV_{\rm AC}}}\frac{dV_{\rm AC}}{dt} = -\frac{1}{2}\frac{W_{bc}}{V_{\rm AC}}\frac{dV_{\rm AC}}{dt}. \tag{28}$$

The base-collector depletion capacitance C_{bc} is given by

$$C_{bc} = \frac{A\varepsilon_{si}}{W_{bc}}. \tag{29}$$

The electron current at the boundary between the depletion layer and the base $(x = W)$ consists of the displacement current of the base-collector junction depletion capacitance and the MOS channel current, and it has the following relationship:

$$I_{mos} + C_{bc}\frac{dV_{\rm AC}}{dt} = I_n(x=W). \tag{30}$$

The MOS channel current can be calculated by [37]

$$I_{\rm mos} = \begin{cases} 0 & ① \\ K_P\left(V_{gs}-V_T-\frac{V_{\rm AC}}{2}\right)V_{\rm AC} & ② \\ \frac{K_P(V_{gs}-V_T)^2}{2} & ③ \end{cases}. \tag{31}$$

The three formulas in (31) correspond to the three situations that ① $V_{gs} \le V_T$, ② $V_{\rm AC} \le V_{gs}-V_T$ and $V_{gs} > V_T$, and ③ $V_{\rm AC} > V_{gs}-V_T$, and $V_{gs} > V_T$, respectively.

The electron current at the collector edge of the base $I_n(x=W)$ can be calculated by (13), as shown in (32) shown at the bottom of next page. Then, the expression of $\frac{dV_{\rm AC}}{dt}$ contains the auxiliary variable P_{L0}, which needs to be eliminated

Based on (6) and (20), the charge stored in the base and the field-stop layer can be obtained, as shown in (33) shown at the bottom of next page. By combining (18), (25), and (33), the relationship between Q and P_{L0} can be obtained

$$P_{L0} = \frac{Q - \frac{W_H^2 I_T}{2D_H}\left(\frac{b_H}{1+b_H}-\frac{b}{1+b}\right)}{qA\left(W_1 + \frac{W_2\tau_H}{V_{\rm AC}}\frac{dV_{\rm AC}}{dt}\right)} \tag{34}$$

where W_1 and W_2 are given by

$$W_1 = W_H + \frac{\cosh\left(\frac{W}{L}\right)-1}{\sinh\left(\frac{W}{L}\right)}L + \frac{DW_H^2\coth\left(\frac{W}{L}\right)}{2D_HL} \tag{35}$$

$$W_2 = \frac{W_H^2W_{bc}}{4D_H\tau_H\sinh\left(\frac{W}{L}\right)}\left[\frac{\cosh\left(\frac{W}{L}\right)+1}{\sinh\left(\frac{W}{L}\right)} - \frac{2L}{W}\right] \tag{36}$$

Using (34), the P_{L0} in the expression of $\frac{dV_{\rm AC}}{dt}$ can be eliminated. The relationship between $\frac{dV_{\rm AC}}{dt}$, $V_{\rm AC}$, I_T, and Q can be obtained by combining (28), (32), and (34), as shown in (37)

$$\frac{b_H}{1+b_H}I_T + qAD_H\frac{P_{HW}-P_{H0}}{W_H} = \frac{b}{1+b}I_T - \frac{qADP_{L0}}{L}\frac{\cosh\left(\frac{W}{L}\right)}{\sin h\left(\frac{W}{L}\right)} + \frac{qAP_{L0}}{\sin h\left(\frac{W}{L}\right)}\frac{dW}{dt}\left[\frac{\cosh\left(\frac{W}{L}\right)+1}{\sin h\left(\frac{W}{L}\right)} - \frac{2L}{W}\right] \tag{24}$$

$$P_{H0} = \frac{W_HI_T}{qAD_H}\left(\frac{b_H}{1+b_H}-\frac{b}{1+b}\right) + P_{L0} + \frac{DW_HP_{L0}}{D_HL}\frac{\cosh\left(\frac{W}{L}\right)}{\sin h\left(\frac{W}{L}\right)} - \frac{W_HP_{L0}}{D_H\sin h\left(\frac{W}{L}\right)}\frac{dW}{dt}\left[\frac{\cosh\left(\frac{W}{L}\right)+1}{\sin h\left(\frac{W}{L}\right)} - \frac{2L}{W}\right]. \tag{25}$$

shown at the bottom of this page. Q_E is given by

$$Q_E = Q - \frac{W_H^2 I_T}{2D_H}\left(\frac{b_H}{1+b_H} - \frac{b}{1+b}\right). \tag{38}$$

It is worth noting that each variable on the right side of (37) can be calculated from the three basic variables $V_{\rm AC}$, Q, and I_T.

Then, it is necessary to obtain the change of charge in the turn-OFF process. There are three main causes for the change in the total charge: the carriers consumed due to the recombination in the base and the field-stop layer, the electrons injected into the emitter, and the electrons injected into the base. Therefore, the change can be calculated as follows [15]:

$$\frac{dQ}{dt} = -I_{nH}\left(x_H = 0\right) + I_n\left(x = W\right) - \frac{Q_H}{\tau_H} - \frac{Q_L}{\tau}. \tag{39}$$

At the emitter-base junction ($x_H = 0$), following the energy band theory, the relationship between the electron current, the junction voltage, and the quasi-Fermi potential of the electrons and holes can be obtained [38], [39]

$$\begin{aligned} I_{nH}(x_H = 0) &= I_{sne}\exp\left(\frac{qV_{eb}}{kT}\right) \\ &= I_{sne}\exp\left[\frac{q\left(\varphi_{pej} - \varphi_{nej}\right)}{kT}\right] \\ &= I_{sne}\exp\left(\frac{E_{Fn} - E_{Fp}}{kT}\right) \\ &= I_{sne}\exp\left(\frac{E_{Fn} - E_{Fi}}{kT}\right)\exp\left(\frac{E_{Fi} - E_{Fp}}{kT}\right) \\ &= \frac{I_{sne}P_{H0}\left(P_{H0} + N_H\right)}{n_i^2}. \end{aligned} \tag{40}$$

Based on (18), (25), (33), and (34), the relationship between Q_H, Q_L, and Q can be obtained by (41) and (42). $\frac{dQ}{dt}$ can be obtained by combining (21), (32), (39)–(42), as shown in (43) shown at the bottom of next page, where P_{H0} can be calculated using (25), (28), and (34), as expressed in (44) shown at the bottom of next page,

$$Q_H = Q - L\frac{\cosh\left(\frac{W}{L}\right) - 1}{\sinh\left(\frac{W}{L}\right)}\frac{Q - \frac{W_H^2 I_T}{2D_H}\left(\frac{b_H}{1+b_H} - \frac{b}{1+b}\right)}{W_1 + \frac{W_2\tau_H}{V_{AC}}\frac{dV_{\rm AC}}{dt}} \tag{41}$$

$$Q_L = L\frac{\cosh\left(\frac{W}{L}\right) - 1}{\sinh\left(\frac{W}{L}\right)}\frac{Q - \frac{W_H^2 I_T}{2D_H}\left(\frac{b_H}{1+b_H} - \frac{b}{1+b}\right)}{W_1 + \frac{W_2\tau_H}{V_{AC}}\frac{dV_{\rm AC}}{dt}} \tag{42}$$

The relationship between the anode-cathode voltage and current flowing through the IGBT in the turn-OFF transient is represented in (37) and (42). On the right side of (37) and (42), each variable can be calculated from V_{AC}, Q, and I_T.

D. Temperature Dependency of the Proposed Model

The temperature dependence of the model is determined by the change of parameters with temperature. These parameters can be divided into two types: silicon physical property parameters (including intrinsic carrier concentration and carrier mobility), and IGBT device parameters (including excess carrier lifetime, emitter electron saturation current, and MOS channel transconductance). These temperature-dependent parameters and the temperature-dependent expressions are given in Table I [40], [41].

The influence of parameter variation with temperature on the electrical behavior of IGBT is demonstrated in Fig. 7. It can be seen from Fig. 7 that, with the increase in temperature, the charge decay rate becomes smaller, which means that the duration of the IGBT turn-OFF phase becomes longer, resulting in an increase in turn-OFF loss. Meanwhile, the increase in temperature also causes the $dV_{\rm AC}/dt$ to become lower, which leads to a longer duration of the turn-OFF stage and a higher turn-OFF loss.

III. Experiment Results

The double pulse test was conducted in this article to verify the accuracy of the proposed model. The equivalent circuit used in the experiment is shown in Fig. 8, where L_d denotes the load inductance, and L_s denotes the stray inductance. The temperature is controlled by a heating platform. In the experiment, the

$$I_n(x = W) = \frac{b}{1+b}I_T - \frac{qADP_{L0}}{L\sinh\left(\frac{W}{L}\right)} + \frac{qAP_{L0}}{\sinh\left(\frac{W}{L}\right)}\frac{dW}{dt}\left[\frac{1 + \cosh\left(\frac{W}{L}\right)}{\sinh\left(\frac{W}{L}\right)} - \frac{2L}{W}\right] \tag{32}$$

$$Q = Q_H + Q_L = \frac{qAW_H\left(P_{HW} + P_{H0}\right)}{2} + \frac{qALP_{L0}}{\sinh\left(\frac{W}{L}\right)}\left[\cosh\left(\frac{W}{L}\right) - 1\right]. \tag{33}$$

$$\begin{aligned} \frac{dV_{AC}}{dt} = &\sqrt{\left(\frac{b_H}{1+b_H}\frac{I_T}{2C_{bc}} - \frac{I_{\rm mos}}{2C_{bc}} - \frac{W_1V_{AC}}{2W_2\tau_H} - \frac{D_HQ}{C_{bc}W_H^2}\right)^2 + \frac{V_{\rm AC}}{W_2\tau_HC_{bc}}\left[W_1\left(\frac{b}{1+b}I_T - I_{\rm mos}\right) - \frac{DQ_E}{L\sinh\left(\frac{W}{L}\right)}\right]} \\ &+ \frac{1}{2C_{bc}}\left(\frac{b_H}{1+b_H}I_T - I_{\rm mos}\right) - \frac{W_1V_{AC}}{2W_2\tau_H} - \frac{D_HQ}{C_{bc}W_H^2}. \end{aligned} \tag{37}$$

TABLE I
TEMPERATURE-DEPENDENT FACTORS

Parameters	Temperature-dependent expression
τ	$\tau(T) = \tau(300\text{ k})(T/300)^{1.7}$
τ_H	$\tau_H(T) = \tau_H(300\text{ k})(T/300)^{1.5}$
μ_n	$\mu_n(T) = 1500(300/T)^{2.5}$
μ_p	$\mu_p(T) = 450(300/T)^{2.5}$
μ_{nH}	$\mu_{nH}(T) = 1200(300/T)^{2.5}$
μ_{pH}	$\mu_{pH}(T) = 410(300/T)^{2.5}$
n_i	$n_i(T) = 3.88 \times 10^{16} T^{1.5}/exp(7000/T)$
I_{sne}	$I_{sne}(T) = \frac{I_{sne}(300\ K)(T/300)^{1.5}}{exp\left[14000\left(\frac{1}{T}-\frac{1}{300}\right)\right]}$
K_p	$K_p(T) = K_p(300\text{ k})(300/T)^{2.5}$

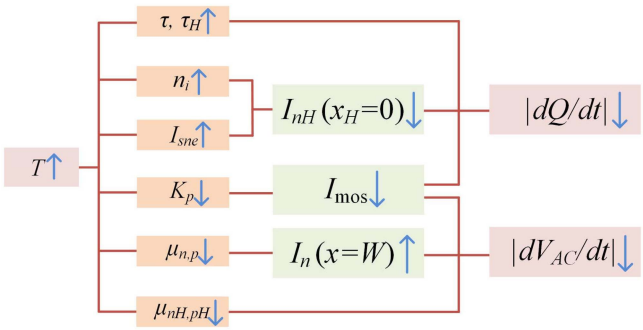

Fig. 7. Details of the temperature dependence of variables.

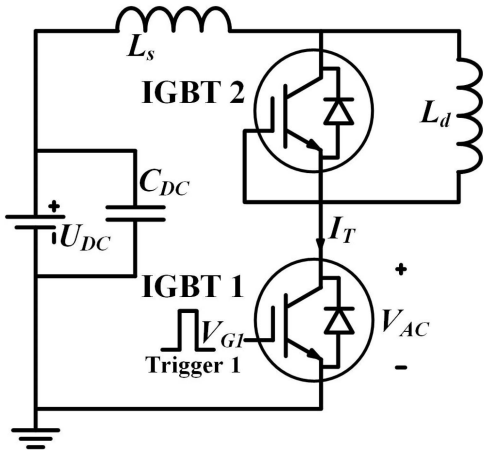

(a)

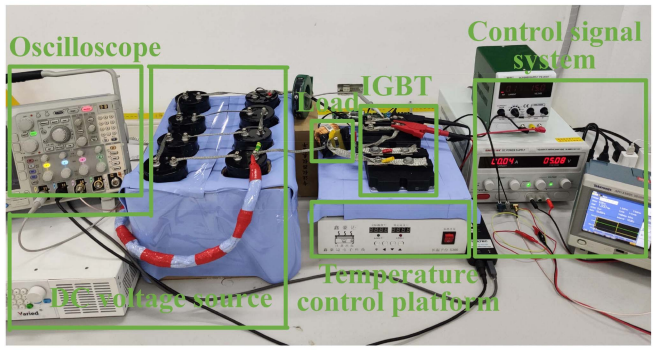

(b)

Fig. 8. IGBT test circuit. (a) Equivalent circuit. (b) Experiment platform.

circuit has a very short working time and is not in a continuous state of operation. Therefore, the influence of IGBT loss on junction temperature can be ignored. The junction temperature and case temperature can be considered to be consistent and controlled by the heating platform. The current passing through the IGBT was measured using the Rogowski coil (Pearson 4997, 0.5 Hz–20 MHz), and the anode-cathode voltage was measured using the differential probe (TESTEC TT-SI 8010B, 0–100 MHz). By changing the value of inductance, temperature, and the conduction time of IGBT, the transient anode-cathode voltage and anode current in the turn-OFF stage with different characteristics can be obtained. Then, the obtained results were compared with the simulation results.

Model parameter extraction is important for utilizing the model. Various methods have been used in this article to extract the required parameters, such as datasheets, optimization algorithms, testing waveforms, etc. [42], [43]. The parameters were obtained by the electrical measurement method, which obtained the highest accuracy among existing methods. Specifically, τ, τ_H, and I_{sne} were obtained according to the current tail decay rate for the clamped inductive load [44], [45], [46]. N_B, N_H, W_b, and W_H were extracted from the relative size of the turn-OFF current tail for the clamped inductive load [44], [45], [46]. K_p was calculated from the IGBT saturation characteristic curve [47], [48]. The extracted model parameters are given in Table II. The tested device used in this article is INFINEON FZ1000R33HE3. The values of the physical constants in the model are given in Table III [49], [50].

Additionally, the parallel diode in the IGBT module will significantly affect the turn-OFF behavior. The transient behavior of the diode has been discussed in detail and comprehensively. In this article, the diode charge-control model is used to investigate the influence of the diode, and the details of the model can be found in reference [51], [52], [53].

$$\frac{dQ}{dt} = -\frac{Q}{\tau_H} + \left(\frac{L}{\tau_H} - \frac{L}{\tau}\right)\frac{\cosh\left(\frac{W}{L}\right)-1}{\sinh\left(\frac{W}{L}\right)}\frac{Q - \frac{W_H^2 I_T}{2D_H}\left(\frac{b_H}{1+b_H} - \frac{b}{1+b}\right)}{W_1 + \frac{W_2\tau_H}{V_{AC}}\frac{dV_{\text{AC}}}{dt}} - \frac{I_{sne}P_{H0}\left(P_{H0}+N_H\right)}{n_i^2} + I_{\text{mos}} + C_{bc}\frac{dV_{\text{AC}}}{dt} \quad (43)$$

$$P_{H0} = \frac{W_H I_T}{qAD_H}\left(\frac{b_H}{1+b_H} - \frac{b}{1+b}\right) + \left[1 + \frac{DW_H}{D_H L}\coth\left(\frac{W}{L}\right) + \frac{2W_2\tau_H}{W_H V_{\text{AC}}}\frac{dV_{\text{AC}}}{dt}\right]\frac{Q - \frac{W_H^2 I_T}{2D_H}\left(\frac{b_H}{1+b_H} - \frac{b}{1+b}\right)}{qA\left(W_1 + \frac{W_2\tau_H}{V_{AC}}\frac{dV_{AC}}{dt}\right)}. \quad (44)$$

TABLE II
PARAMETER VALUES OF THE TESTED IGBT ($T = 300$ K)

Parameters	Values	Parameter Extraction Method [44], [45], [46], [47], [48]
τ	6.6 μs	Electrical measurement [44], [45], [46] (The current tail decay rate)
τ_H	0.2 μs	
I_{sne}	1.63×10^{-13} A	
N_B	2×10^{13} cm^{-3}	Electrical measurement [44], [45], [46] (The relative size of the turn-off current tail)
N_H	1.8×10^{16} cm^{-3}	
W_b	340 μm	
W_H	20 μm	
K_p	60 A/V^2	Electrical measurement [47], [48] (IGBT saturation characteristic curve)

TABLE III
PARAMETER VALUES OF SILICON ($T = 300$ K) [49], [50]

Parameters	Values
μ_n	1500 cm^2/V·s
μ_p	450 cm^2/V·s
μ_{nH}	1200 cm^2/V·s
μ_{pH}	410 cm^2/V·s
n_i	1.45×10^{10} cm^{-3}
ε_{si}	1.05×10^{-12} F/cm

The anode-cathode voltage and anode current in the turn-OFF stage were measured under a certain temperature T (25/75/125 °C), load inductor L_d (4.5/6/35 uH), dc voltage $U_{\rm DC}$ (1000/1500/2000 V), and switching current $I_{T\max}$ (the maximum current in the turn-OFF stage, 100/500/1000 A), and the measurement results were compared with the simulation results calculated by the proposed model, as shown in Figs. 9, 10, and 11. The Hefner model was chosen as a representative, which is based on the first-order approximation and does not consider the effect of carrier recombination.

As shown in Figs. 9, 10, and 11, at different temperatures, the simulation waveforms obtained from the proposed model are highly consistent with the experimental data. Compared with the existing model, the proposed model has a faster current decline rate and voltage rise rate in the turn-OFF stage, which is more consistent with the experimental data. This indicates that the loss in the turn-OFF stage calculated by the current model will be higher. Compared with the existing model, the proposed model considers the effect of carrier recombination, so the excess carriers stored in the base region and the field-stop layer will be depleted faster. This is because the proposed model is more consistent with the actual physical process than the Hefner model. With the decrease in the switching current, the oscillation of the switching current becomes more severe, and the error between the simulation and experiment tends to increase, but it is within an acceptable range.

As the temperature increases, the duration of the turn-OFF phase becomes longer under the same operating conditions, which is consistent with the analysis result in Section II. Meanwhile, with the increase in the switching current, the anode-cathode voltage overshoot becomes higher and the duration of the turn-OFF stage also increases.

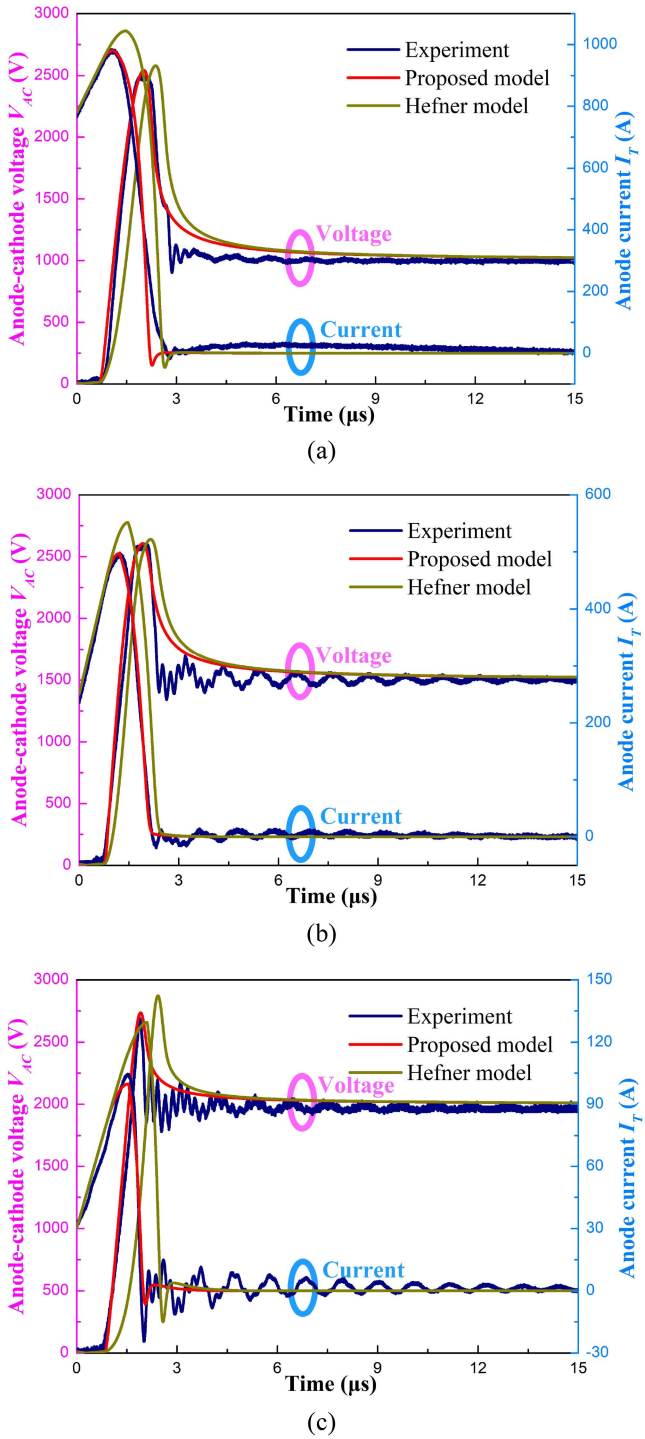

Fig. 9. Simulation and testing waveforms at $T = 25$ °C. (a) $U_{\rm DC} = 1000$ V, $I_{T\max} \cong 1000$ A, and $L_d = 4.5$ μH. (b) $U_{\rm DC} = 1500$ V, $I_{T\max} \cong 500$ A, and $L_d = 6$ μH, (c) $U_{\rm DC} = 2000$ V, $I_{T\max} \cong 100$ A, and $L_d = 35$ μH.

The turn-OFF loss of the IGBT is a major concern in most applications. Therefore, the accuracy of simulating the turn-OFF loss of the proposed model is further investigated. The comparison between the turn-OFF loss calculated by the proposed model, obtained by experiments and calculated by the existing model are given in Table IV. It is worth noting that although the duration of the turn-OFF phase increases with the temperature, the measured turn-OFF loss does not simply show an increasing trend with the

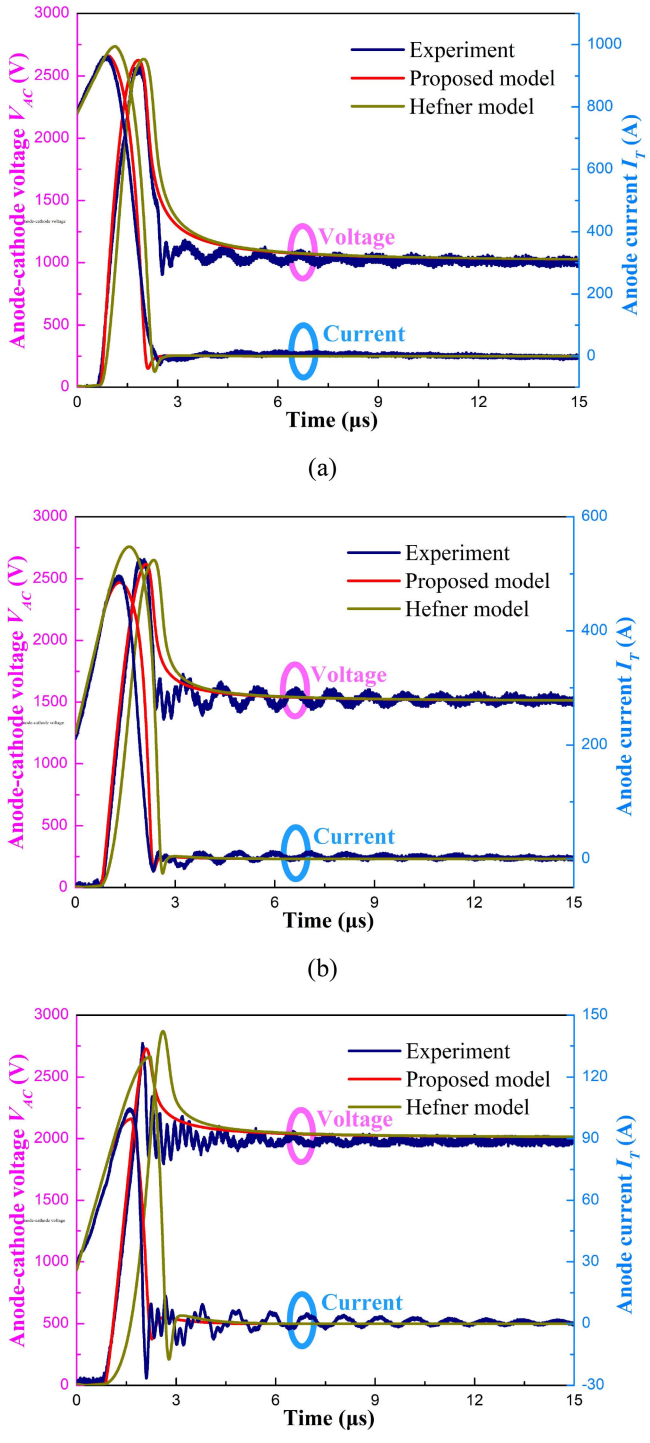

Fig. 10. Simulation and testing waveforms at $T = 75$ °C. (a) $U_{\rm DC} = 1000$ V, $I_{T\rm max} \cong 1000$ A, and $L_d = 4.5$ μH, (b) $U_{\rm DC} = 1500$ V, $I_{T\rm max} \cong 500$ A, and $L_d = 6$ μH, (c) $U_{\rm DC} = 2000$ V, $I_{T\rm max} \cong 100$ A, and $L_d = 35$ μH.

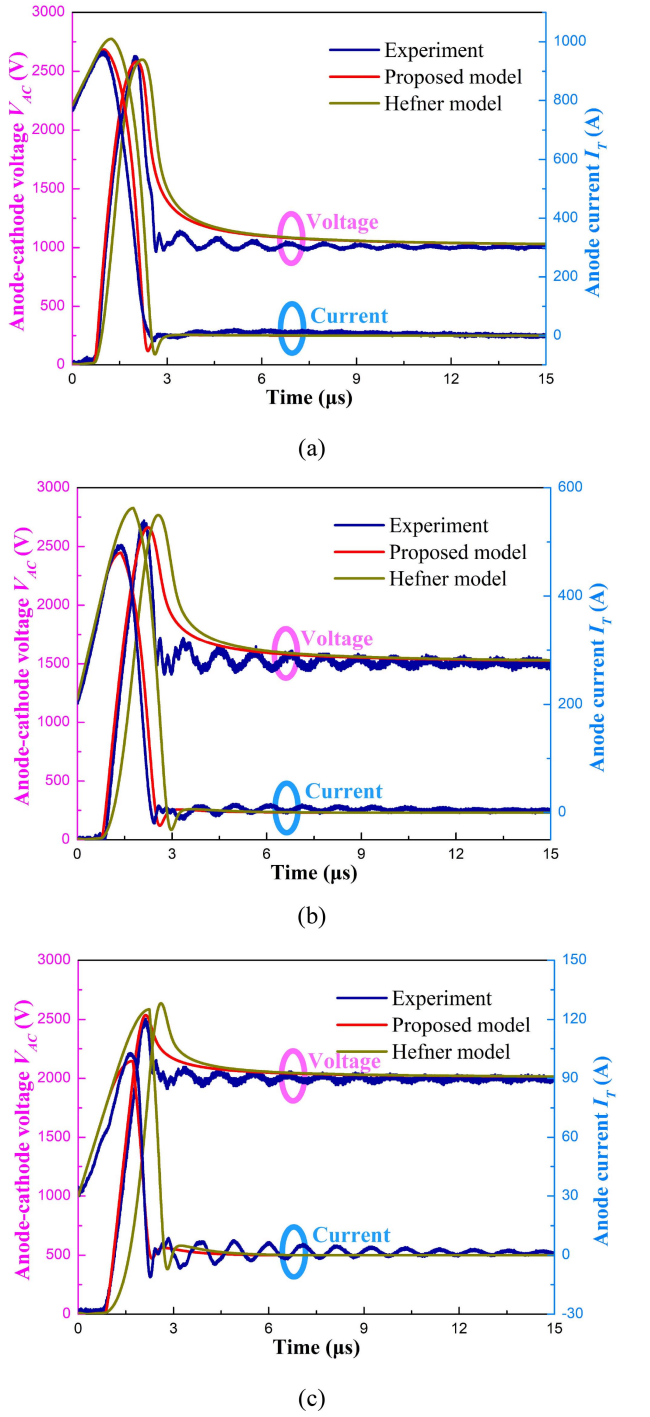

Fig. 11. Simulation and testing waveforms at $T = 125$ °C. (a) $U_{\rm DC} = 1000$ V, $I_{T\rm max} \cong 1000$ A, and $L_d = 4.5$ μH, (b) $U_{\rm DC} = 1500$ V, $I_{T\rm max} \cong 500$ A, and $L_d = 6$ μH. (c) $U_{\rm DC} = 2000$ V, $I_{T\rm max} \cong 100$ A, and $L_d = 35$ μH.

temperature. There are two main reasons for this phenomenon. One is the influence of parasitic effects: temperature will affect the parasitic effects of the circuit, and this influence is difficult to predict. The other is the influence of temperature on other components in the circuit. To suppress the influence of stray parameters on the evaluation of model accuracy, the length of the connecting wires between devices should be decreased as much as possible in the experiment. Therefore, in the double-pulse experiment, the entire experiment circuit was placed on the temperature control platform. Temperature also affects the electrical behavior of other devices. Due to these processes, the characteristics of the turn-OFF loss of the IGBT are complicated.

TABLE IV
TURN-OFF LOSS OF FIGS. 9, 10, AND 11

Number of pictures	Experiment	Proposed model	Hefner model
Fig. 9(a)	1.703 J	1.672 J	1.894 J
Fig. 9(b)	0.812 J	0.798 J	0.928 J
Fig. 9(c)	0.121 J	0.130 J	0.171 J
Fig. 10(a)	1.622 J	1.600 J	1.780 J
Fig. 10(b)	0.947 J	0.970 J	1.114 J
Fig. 10(c)	0.142 J	0.152 J	0.195 J
Fig. 11(a)	1.813 J	1.862 J	1.987 J
Fig. 11(b)	0.918 J	0.935 J	1.147 J
Fig. 11(c)	0.153 J	0.148 J	0.186 J

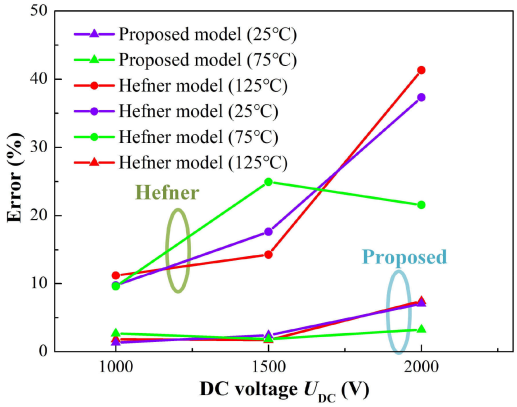

Fig. 12. Comparison of the relative errors.

The comparison between the relative errors of the proposed model and those calculated by the Hefner model is shown in Fig. 12. The turn-OFF loss calculated by the Hefner model is much larger than that obtained by the double pulse test, with a relative error of 9.6%–40.3%. The turn-OFF loss calculated by the model proposed in this article is much more accurate, and the relative error does not exceed 7.4%. In the initial stage of the turn-OFF process, the anode-cathode voltage and anode current are high, and the loss in this stage accounts for most of the turn-OFF loss. Compared with the Hefner model, the anode-cathode voltage and anode current calculated by the proposed model are more consistent with the experimental results, so the loss prediction is more accurate. Moreover, since the recombination of carriers is not considered in the Hefner model, which leads to a slower depletion of excess carriers stored in the base and the field-stop layer, the turn-OFF loss calculated by the Hefner model is larger

A comparison of the above aspects indicates that the consideration of the effect of carrier recombination improves the modeling accuracy significantly. Compared with the Hefner model, the proposed model improves the accuracy of predicting the turn-OFF characteristics of the high-voltage IGBT significantly. The error between the results calculated by the proposed model and those obtained by experiments falls within an acceptable low range.

IV. CONCLUSION

This article presents a new analytical transient model for the turn-OFF process of high-voltage IGBTs. First, the defect of the existing model used in high-voltage IGBTs is analyzed in detail. Then, by considering the effect of carrier recombination and based on the hyperbolic approximation of carrier distribution, the transient ADE is solved analytically. Finally, the accuracy of the proposed model is verified by comparing the experimental and simulated turn-OFF waveforms under different temperatures, bus voltage, and switching current. Results show that the proposed model has significantly higher accuracy than the existing model. Future work will focus on the improvement of approximation methods and consider multidimensional processes to further improve the accuracy of the model.

REFERENCES

[1] A. S. Bahman, K. Ma, and F. Blaabjerg, "A lumped thermal model including thermal coupling and thermal boundary conditions for high power IGBT modules," *IEEE Trans. Power Electron.*, vol. 33, no. 3, pp. 2518–2530, Mar. 2018, doi: 10.1109/TPEL.2017.2694548.

[2] Z. Zeng, J. Wang, F. Li, X. Yin, and Z. J. Shen, "Modeling and analysis of a new pressure contact package for high-current large-die IGBTs," *IEEE J. Emerg. Sel. Topics Power Electron.*, vol. 7, no. 3, pp. 1615–1626, Sep. 2019, doi: 10.1109/JESTPE.2019.2921012.

[3] H. Bai, C. Liu, A. K. Rathore, D. Paire, and F. Gao, "An FPGA-based IGBT behavioral model with high transient resolution for real-time simulation of power electronic circuits," *IEEE Trans. Ind. Electron.*, vol. 66, no. 8, pp. 6581–6591, Aug. 2019, doi: 10.1109/TIE.2018.2870354.

[4] R. Wu, F. Blaabjerg, H. Wang, M. Liserre, and F. Iannuzzo, "Catastrophic failure and fault-tolerant design of IGBT power electronic converters—An overview," in *Proc. IECON*, Nov. 2013, pp. 507–513.

[5] L. L. Foro et al., "Gate voltage contribution to neutron-induced SEB of trench Gate fieldstop IGBT," *IEEE Trans. Nucl. Sci.*, vol. 61, no. 4, pp. 1739–1746, Aug. 2014, doi: 10.1109/TNS.2014.2332813.

[6] X. Liu, L. Wang, G. Liang, and L. Qi, "Modeling turn-off process of high-power IGBT based on both quasi static and nonquasi static assumptions," *IEEE Trans. Power Electron.*, vol. 37, no. 10, pp. 12197–12208, Oct. 2022, doi: 10.1109/TPEL.2022.3178217.

[7] X. Yang, Y. Ding, J. Wang, G. Liu, and P. R. Palmer, "An improved Fourier-series-based IGBT model by mitigating the effect of Gibbs phenomenon at turn on," *IEEE Trans. Electron Devices*, vol. 68, no. 7, pp. 3453–3459, Jul. 2021, doi: 10.1109/TED.2021.3077204.

[8] P. Xue and P. Davari, "A temperature-dependent dV_{CE}/dt model for field-stop IGBT at turn-off transient," *IEEE J. Emerg. Sel. Topics Power Electron.*, vol. 11, no. 3, pp. 3173–3183, Jun. 2023, doi: 10.1109/JESTPE.2023.3243856.

[9] K. Sheng, B. W. Williams, and S. J. Finney, "A review of IGBT models," *IEEE Trans. Power Electron*, vol. 15, no. 6, pp. 1250–1266, Nov. 2000, doi: 10.1109/63.892840.

[10] Y. Xu, C. N. M. Ho, A. Ghosh, and D. Muthumuni, "An electrical transient model of IGBT-diode switching cell for power semiconductor loss estimation in electromagnetic transient simulation," *IEEE Trans. Power Electron.*, vol. 35, no. 3, pp. 2979–2989, Mar. 2020, doi: 10.1109/TPEL.2019.2929113.

[11] D. L. Scharfetter and A. G. Jordan, "Reactive effects in semiconductor filaments due to conductivity modulation and an extension of the theory of the double-base diode," *IRE Trans. Electron Devices*, vol. 9, no. 6, pp. 461–473, Nov. 1962.

[12] I. Son, W. Tang, and D. H. Navon, "Modeling of bistable device I-V characteristic resulting from conductivity modulation in semiconductors," *IEEE Trans. Electron Devices*, vol. 35, no. 4, pp. 450–458, Apr. 1988.

[13] J. K. O. Sin, C. A. T. Salama, and L. Hou, "The SINFET—A Schottky injection MOS-gated power transistor," *IEEE Trans. Electron Devices*, vol. 33, no. 12, pp. 1940–1947, Dec. 1986.

[14] J. K. O. Sin, C. A. T. Salama, and L. Z. Hou, "Transient characteristics of n-channel hybrid Schottky injection FETs," *IEEE Trans. Electron Devices*, vol. 36, no. 5, pp. 993–1000, May 1989.

[15] A. R. Hefner and D. L. Blackburn, "An analytical model for the steady-state and transient characteristics of the power insulated-gate bipolar transistor," *Solid-State Electron.*, vol. 31, no. 10, pp. 1513–1532, Oct. 1988, doi: 10.1016/0038-1101(88)90025-1.
[16] A. R. Hefner and D. M. Diebolt, "An experimentally verified IGBT model implemented in the Saber circuit simulator," *IEEE Trans. Power Electron*, vol. 9, no. 5, pp. 532–542, Sep. 1994, doi: 10.1109/63.321038.
[17] S. Ji, Z. Zhao, and T. Lu, "HVIGBT physical model analysis during transient," *IEEE Trans. Power Electron.*, vol. 28, no. 5, pp. 2616–2624, May 2013, doi: 10.1109/TPEL.2012.2218620.
[18] S. Ji, T. Lu, and Z. Zhao, "Physical model analysis during transient for series-connected HVIGBTs," *IEEE Trans. Power Electron.*, vol. 29, no. 11, pp. 5727–5737, Nov. 2014, doi: 10.1109/TPEL.2014.2300104.
[19] Y. Luo, F. Xiao, B. Liu, and Y. Huang, "A physics-based transient electrothermal model of high-voltage press-pack IGBTs under HVdc interruption," *IEEE Trans. Power Electron.*, vol. 35, no. 6, pp. 5660–5669, Jun. 2020, doi: 10.1109/TPEL.2019.2948936.
[20] R. Kraus and K. Hoffmann, "An analytical model of IGBT's with low emitter efficiency," in *Proc. 5th Int. Symp. Power Semicond. Devices ICs*, May 1993, vol. 3, pp. 30–34, doi: 10.1109/ISPSD.1993.297102.
[21] R. Kraus, P. Turkes, and J. Sigg, "Physics-based models of power semiconductor devices for the circuit simulator SPICE," in *Proc. IEEE29th Annu. IEEE Power Electron. Specialists Conf.*, May 1998, vol. 2, pp. 1726–1731, doi: 10.1109/PESC.1998.703414.
[22] P. O. Lauritzen and C. L. Ma, "A simple diode model with reverse recovery," *IEEE Trans. Power Electron.*, vol. 6, no. 2, pp. 188–191, Apr. 1991, doi: 10.1109/63.76804.
[23] F. Iannuzzo and G. Busatto, "Physical CAD model for high-voltage IGBTs based on lumped-charge approach," *IEEE Trans. Power Electron.*, vol. 19, no. 4, pp. 885–893, Jul. 2004, doi: 10.1109/TPEL.2004.830085.
[24] Y. Duan, F. Xiao, Y. Luo, and F. Iannuzzo, "A lumped-charge approach based physical SPICE-model for high power soft-punch through IGBT," *IEEE J. Emerg. Sel. Topics Power Electron.*, vol. 7, no. 1, pp. 62–70, Mar. 2019, doi: 10.1109/JESTPE.2018.2874105.
[25] Y. Duan, F. Iannuzzo, and F. Blaabjerg, "A new lumped-charge modeling method for power semiconductor devices," *IEEE Trans. Power Electron.*, vol. 35, no. 4, pp. 3989–3996, Apr. 2020, doi: 10.1109/TPEL.2019.2938104.
[26] P. Leturcq, M. O. Berraies, and J. -. Massol, "Implementation and validation of a new diode model for circuit simulation," in *Proc. Annu. IEEE Power Electron. Specialists Conf.*, 1996, vol. 1, pp. 35–43, doi: 10.1109/PESC.1996.548556.
[27] P. R. Palmer, E. Santi, J. L. Hudgins, X. Kang, J. C. Joyce, and P. Y. Eng, "Circuit simulator models for the diode and IGBT with full temperature dependent features," *IEEE Trans. Power Electron.*, vol. 18, no. 5, pp. 1220–1229, Sep. 2003, doi: 10.1109/TPEL.2003.816194.
[28] A. T. Bryant, L. Lu, E. Santi, J. L. Hudgins, and P. R. Palmer, "Modeling of IGBT resistive and inductive turn-on behavior," *IEEE Trans. Ind. Appl.*, vol. 44, no. 3, pp. 904–914, May–Jun. 2008, doi: 10.1109/TIA.2008.921384.
[29] L. Lu, A. Bryant, J. L. Hudgins, P. R. Palmer, and E. Santi, "Physics-based model of planar-gate IGBT including MOS side two-dimensional effects," *IEEE Trans. Ind. Appl.*, vol. 46, no. 6, pp. 2556–2567, Nov.-Dec. 2010, doi: 10.1109/TIA.2010.2071190.
[30] A. Bryant et al., "Investigation into IGBT dV/dt during turn-off and its temperature dependence," *IEEE Trans. Power Electron.*, vol. 26, no. 10, pp. 3019–3031, Oct. 2011, doi: 10.1109/TPEL.2011.2125803.
[31] Y. Ding, X. Yang, J. Wang, C. Tu, and G. Liu, "Investigation on parameter extraction for an improved Fourier-series-based NPT IGBT model," in *Proc. IEEE Workshop Wide Bandgap Power Devices Appl. Asia*, 2021, pp. 51–56, doi: 10.1109/WiPDAAsia51810.2021.9656041.
[32] Y. Ding, X. Yang, G. Liu, and J. Wang, "Physics-based trench-gate field-stop IGBT modeling with optimization-based parameter extraction for device parameters," *IEEE Trans. Electron Devices*, vol. 68, no. 12, pp. 6305–6312, Dec. 2021, doi: 10.1109/TED.2021.3120691.
[33] R. Bonyadi et al., "Physics-based modelling and experimental characterisation of parasitic turn-on in IGBTs," in *Proc. Eur. Conf. Power Electron. Appl.*, 2015, pp. 1–9, doi: 10.1109/EPE.2015.7309179.
[34] P. Xue, G. Fu, and D. Zhang, "Modeling inductive switching characteristics of high-speed buffer layer IGBT," *IEEE Trans. Power Electron.*, vol. 32, no. 4, pp. 3075–3087, Apr. 2017, doi: 10.1109/TPEL.2016.2570838.
[35] Y. Luo, F. Xiao, B. Liu, and Y. Huang, "A physics-based transient electrothermal model of high-voltage press-pack IGBTs under HVdc interruption," *IEEE Trans. Power Electron.*, vol. 35, no. 6, pp. 5660–5669, Jun. 2020, doi: 10.1109/TPEL.2019.2948936.
[36] W. Shockley, *Electrons and Holes in Semicondcutors*, New York, NY, USA: Van Nostrand, 1956.
[37] K. Chen, Z. Zhao, L. Yuan, T. Lu, and F. He, "The impact of nonlinear junction capacitance on switching transient and its modeling for SiC MOSFET," *IEEE Trans. Electron. Devices*, vol. 62, no. 2, pp. 333–338, Feb. 2015, doi: 10.1109/TED.2014.2362657.
[38] X. Kang, A. Caiafa, E. Santi, J. L. Hudgins, and P. R. Palmer, "Characterization and modeling of high-voltage field-stop IGBTs," *IEEE Trans. Ind. Appl.*, vol. 39, no. 4, pp. 922–928, Jul./Aug. 2003, doi: 10.1109/TIA.2003.814547.
[39] A. R. Hefner, "Modeling buffer layer IGBTs for circuit simulation," *IEEE Trans. Power Electron.*, vol. 10, no. 2, pp. 111–123, Mar. 1995, doi: 10.1109/63.372596.
[40] A. R. Hefner, "A dynamic electro-thermal model for the IGBT," *IEEE Trans. Power Electron.*, vol. 30, no. 2, pp. 394–405, Apr. 1994, doi: 10.1109/28.287517.
[41] Y. Chen, H. Luo, W. Li, X. He, F. Iannuzzo, and F. Blaabjerg, "Analytical and experimental investigation on A dynamic thermo-sensitive electrical parameter with maximum dI_C/dt during turn-off for high power trench gate/field-stop IGBT modules," *IEEE Trans. Power Electron.*, vol. 32, no. 8, pp. 6394–6404, Aug. 2017, doi: 10.1109/TPEL.2016.2619620.
[42] A. T. Bryant, X. Kang, E. Santi, P. R. Palmer, and J. L. Hudgins, "Two-step parameter extraction procedure with formal optimization for physics-based circuit simulator IGBT and p-i-n diode models," *IEEE Trans. Power Electron*, vol. 21, no. 2, pp. 295–309, Mar. 2006, doi: 10.1109/TPEL.2005.869742.
[43] R. Chibante, A. AraÚjo, and A. Carvalho, "Finite-element modeling and optimization-based parameter extraction algorithm for NPT-IGBTs," *IEEE Trans. Power Electron*, vol. 24, no. 5, pp. 1417–1427, May 2009, doi: 10.1109/TPEL.2009.2012388.
[44] A. R. Hefner, "Modeling buffer layer IGBTs for circuit simulation," *IEEE Trans. Power Electron.*, vol. 10, no. 2, pp. 111–123, Mar. 1995, doi: 10.1109/63.372596.
[45] M. A. Rodríguez et al., "Reconfigurable Special Test circuit of physics-based IGBT models parameter extraction," *Solid-State Electron*, vol. 54, no. 11, pp. 1246–1256, 2010.
[46] G. Fu and P. Xue, "An excess carrier lifetime extraction method for physics-based IGBT models," *J. Power Electron.*, vol. 16, no. 2, pp. 778–785, 2016.
[47] A. Claudio, M. Cotorogea, and M. A. Rodriguez, "Parameter extraction for physics-based IGBT models by electrical measurements," in *Proc. IEEE 33rd Annu. IEEE Power Electron. Specialists Conf.*, 2002, vol. 3, pp. 1295–1300, doi: 10.1109/PSEC.2002.1022355.
[48] G. Feng, Z. Zhao, L. Yuan, S. Ji, and J. Zhao, "Research on HVIGBT transient mixture model and parameter extraction method," in *Proc. IEEE Conf. Expo Transp. Electrific. Asia-Pac.*, 2014, pp. 1–6, doi: 10.1109/ITEC-AP.2014.6940694.
[49] C. Lombardi, S. Manzini, A. Saporito, and M. Vanzi, "A physically based mobility model for numerical simulation of nonplanar devices," *IEEE Trans. Comput.-Aided Des. Integr. Circuits Syst.*, vol. 7, no. 11, pp. 1164–1171, Nov. 1988, doi: 10.1109/43.9186.
[50] V. K. Khanna, *Insulated Gate Bipolar Transistor IGBT Theory and Design*. Hoboken, NJ, USA: Wiley, 2003.
[51] C. L. Ma and P. O. Lauritzen, "A simple power diode model with forward and reverse recovery," *IEEE Trans. Power Electron*, vol. 8, no. 4, pp. 342–346, Oct. 1993, doi: 10.1109/63.261002.
[52] X. Li, Y. Luo, Y. Duan, Y. Huang, and B. Liu, "A lumped-charge model for high-power PT-p-i-n diode with a buffer layer," *IEEE J. Emerg. Sel. Topics Power Electron.*, vol. 7, no. 1, pp. 52–61, Mar. 2019, doi: 10.1109/JESTPE.2019.2894783.
[53] Y. Duan, F. Xiao, Y. Jia, Y. Luo, and B. Liu, "A physics-based lumped-charge model for SiC MPS diode implemented in PSPICE," *IEEE J. Emerg. Sel. Topics Power Electron.*, vol. 7, no. 3, pp. 1547–1555, Sep. 2019, doi: 10.1109/JESTPE.2019.2923823.

Zhiyuan Zhang was born in Anhui, China, in 1996. He received the B.S. degree in 2018 from Huazhong University of Science and Technology, Wuhan, China, where he is currently working toward the Ph.D. degree with the High Voltage Division, School of Electrical and Electronic Engineering, State Key Laboratory of Advanced Electromagnetic Engineering and Technology.

His research interests include semiconductor device, high voltage converter and lightning protection.

Hengxin He (Member, IEEE) was born in Chongqing city, China, in 1982. He received the B.S., Master's, and Ph.D. degrees in electrical engineering from Huazhong University of Science and Technology, Wuhan, China, in 2005, 2007, and 2012, respectively.

He is currently an Associate Professor with the State Key Laboratory of Advanced Electromagnetic Engineering and Technology, HUST. His research interests include the lightning physics, plasma diagnosis, the insulation and coordination of power system.

Kejie Li (Member, IEEE) was born in Shanxi, China, in 1989. He received the B.S. and Ph.D. degrees in electrical engineering from Xi'an Jiaotong University, Xi'an, China, in 2012 and 2019, respectively.

He is currently a Post-Doctoral Researcher with the School of Electrical Engineering and Automation, Hefei University of Technology, Hefei, China. His research interests include modeling and calculation for electromagnetic transients, electromagnetic pulse generation and measurement, and electromagnetic susceptibility test and evaluation.

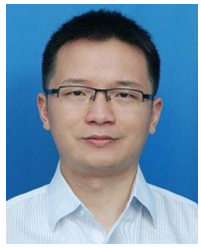

Nianwen Xiang (Member, IEEE) was born in Hubei, China, in 1985. He received the B.S. and M.S. degrees in electrical and electronics engineering from Wuhan University, Wuhan, China, in 2007 and 2009, respectively, and the Ph.D. degree in electrical and electronics engineering from North China Electric Power University, Beijing, China, in 2017.

He is currently a Professor with the School of Electrical Engineering and Automation, Hefei University of Technology, Hefei, China. His research interests include lightning protection and grounding, and high-voltage testing technology.

Weijiang Chen (Senior Member, IEEE) was born in Shandong Province, China, in 1958. He received the B.Sc. degree in electrical engineering from Hefei University of Technology, Hefei, China, and the M.Sc. degree in electrical engineering from China Electric Power Research Institute (CEPRI), Beijing, China, in 1982 and 1985, respectively.

From 1985 to 2005, he was a Professor with CEPRI. He was the President of the High Voltage Research Department from 1995 to 2000, the Vice President of CEPRI from 2000 to 2005, and the President of Wuhan High Voltage Research Institute, from 2005 to 2008. He has been the Vice Director of UHV Department of State Grid Corporation of China (SGCC) since 2008, taking charge of constructing UHV transmission lines of SGCC. He is the author of many books and technical papers. He was appointed as the president of IEEE-SA UHV Working Groups in 2011, forming three IEEE standards. His research interests include overvoltage protection, ultrahigh voltage transmission, insulation coordination, surge arrester, and electromagnetic environment in power system.

Prof. Chen is the Chairman of HV Professional Committee of Chinese Society for Electrical Engineering and Chairman of China EMC Standardization Technology Committee, has been recommended as the Chief Editor of the journal High Voltage which is co-published by IET and the China Electric Power Research Institute.